

Surveying structural complexity in quantum many-body systems

Whei Yeap Suen,^{1,*} Thomas J. Elliott,^{2,3,†} Jayne Thompson,¹ Andrew J. P. Garner,^{4,1} John R. Mahoney,⁵ Vlatko Vedral,^{6,1,7} and Mile Gu^{3,2,1,‡}

¹*Centre for Quantum Technologies, National University of Singapore, 3 Science Drive 2, Singapore 117543*

²*Complexity Institute, Nanyang Technological University, Singapore 637335*

³*School of Mathematical and Physical Sciences, Nanyang Technological University, Singapore 637371*

⁴*Institute for Quantum Optics and Quantum Information, Austrian Academy of Sciences, Boltzmannngasse 3, A-1090 Vienna, Austria*

⁵*Complexity Sciences Center and Physics Department, University of California at Davis, One Shields Avenue, Davis, California 95616, USA*

⁶*Department of Physics, Clarendon Laboratory, University of Oxford, Parks Road, Oxford, OX1 3PU, United Kingdom.*

⁷*Department of Physics, National University of Singapore, 3 Science Drive 2, Singapore 117543*

(Dated: December 31, 2018)

Quantum many-body systems exhibit a rich and diverse range of exotic behaviours, owing to their underlying non-classical structure. These systems present a deep structure beyond those that can be captured by measures of correlation and entanglement alone. Using tools from complexity science, we characterise such structure. We investigate the structural complexities that can be found within the patterns that manifest from the observational data of these systems. In particular, using two prototypical quantum many-body systems as test cases – the one-dimensional quantum Ising and Bose-Hubbard models – we explore how different information-theoretic measures of complexity are able to identify different features of such patterns. This work furthers the understanding of full-quantum notions of structure and complexity in quantum systems and dynamics.

I. INTRODUCTION

Quantum many-body systems hold a distinguished position in modern physics, playing a vital role in providing insight into the physical world. On the one hand, they constitute an excellent platform for studying a range of phenomena through their utility in quantum simulation [1–4]. Conversely, the properties intrinsic to these systems are interesting in their own right, and they thus form a target of simulation and modelling themselves [5–12]. Understanding the structures present in these systems, and the resources needed to characterise, study and emulate them, is thus of paramount importance.

Quantum entanglement [13, 14] captures the quantum correlations present in a system, and so plays a significant role in identifying structure in quantum systems. In particular, the *half-chain entanglement* quantifies the amount of information shared between the left and right halves of a one-dimensional quantum system; it provides an indicator to the amount of classical resources needed to simulate such systems [15–18], and related quantum mutual information-based quantities have previously been associated with structural complexity [19]. Nevertheless, complex systems possess structure beyond such correlations; we turn to tools from complexity science to identify and quantify this structure. The field of *computational mechanics* [20–22] adopts an information-theoretic approach to this task, and equates struc-

ture in a stochastic process with the minimal amount of information that must be stored by a model that replicates its behaviour. Moreover, it offers a systematic approach to determining such minimal models.

Impelled by the growth of quantum technologies, recent efforts have extended the computational mechanics framework into the quantum regime, finding that classical limits on the information that models must store can be overcome [23–30]. This fundamentally changes how we might perceive and characterise structure – two prominent examples being the ambiguities of simplicity [31–33] and optimality [30, 34], which highlight properties of complexity that might be considered truisms classically no longer hold in the quantum domain. Practically, these quantum models can provide memory savings for stochastic simulation, and the resource gap between minimal quantum and classical simulators can even grow unbounded [28, 29, 35–37].

It is natural then to ask how these measures of complexity look – and what they can tell us about structure – when applied to quantum many-body systems. In this article, we apply this framework to study their structure and complexity. To this end, we look at the structure manifest in the measurement statistics of quantum states. This serves as a crucial first step in identifying the structure in the quantum processes that gave rise to the states. We begin by reviewing in Section II the relevant details of causal models and measures of complexity that form the background to our work. In Section III, we introduce the mapping from states of quantum chains to stochastic processes through the statistics of observation sequences, and apply it to quantify structure in the one-dimensional quantum Ising and Bose-Hubbard models. We discuss the implications of our results and the future directions

*Electronic address: wheiyeap@u.nus.edu

†Electronic address: physics@tjelliott.net

‡Electronic address: cqtmileg@nus.edu.sg

to which our framework may be applied in Section IV.

II. FRAMEWORK

Stochastic processes. We consider discrete-event, discrete-time stationary stochastic processes [38]. At each timestep $t \in \mathbb{Z}$ such a process emits a symbol r_t drawn from a configuration space \mathcal{R} . We use R_t to denote the random variable governing output r_t . We also designate the semi-infinite strings $\vec{R}_t := \dots R_{t-1}R_t$ and $\vec{\bar{R}}_t := R_{t+1}R_{t+2}\dots$ as the random variables associated with the past and future observation sequences $\vec{r}_t := \dots r_{t-1}r_t$ and $\vec{r}'_t := r_{t+1}r_{t+2}\dots$ at time t respectively (throughout, upper case indicates random variables, and lower case the corresponding variates). The output symbol statistics are then described by a conditional probability distribution over these strings $P(\vec{R}_t|\vec{\bar{R}}_t)$, detailing how future observations are correlated with past observations. We use the notation $r_{t:t+n} = r_t r_{t+1} \dots r_{t+n-1}$ to represent the sequence of outputs between t and $t+n-1$. Stationarity of a stochastic process is defined by $P(R_{0:n}) = P(R_{L:L+n}) \forall n, L \in \mathbb{Z}$; this allows us to drop the subscript t from semi-infinite strings.

Causal models. A *causal model* of a stationary stochastic process [20, 21, 37] is tasked with replicating its future output statistics according to the distribution $P(\vec{R}|\vec{\bar{R}})$; it stores information about the past of a stochastic process in its internal memory, and uses this to predict the future output statistics. Crucially, a causal model contains no information about the future that cannot be inferred from the past (i.e., the mutual information between the memory and future outputs given the past outputs is zero). Causal models use an encoding function f to map pasts \vec{r} to states $m \in \mathcal{M}$ according to $m = f(\vec{r})$, such that $P(\vec{R}|m = f(\vec{r})) = P(\vec{R}|\vec{r})$. At each timestep t , the model produces an output r following $P(R_{t+1} = r|m_t) = P(R_{t+1} = r|\vec{r}_t)$. At time $t+1$, r becomes part of the past observation sequence, and the memory state is updated to $m_{t+1} = f(\vec{r}')$, where the new past $\vec{r}' = \vec{r}r$ is the concatenation of the previous past with the new output symbol. The information stored by such a model is given by the Shannon entropy of its set of internal memory states:

$$H(M) = \sum_{m \in \mathcal{M}} -P_m \log P_m, \quad (1)$$

where $P_m = \sum_{\vec{r} \in m} P(\vec{r})$.

For any given stationary stochastic process, one can construct myriad causal models of the process that will faithfully replicate the future statistics. The field of computational mechanics provides us with a systematic way to identify and construct the provably optimal classical causal model of a given process [20–22]. By optimal, we here mean the model that stores the least possible amount of past information [Eq. (1)] while accurately simulating the process; the optimal classical causal model

is referred to as the ε -machine. In this framework, sets of pasts are grouped into equivalence classes called *causal states* according to the relation

$$\vec{r} \sim_e \vec{r}' \iff P(\vec{R} = \vec{r}|\vec{\bar{R}} = \vec{r}) = P(\vec{R} = \vec{r}'|\vec{\bar{R}} = \vec{r}') \forall \vec{r}. \quad (2)$$

Eq. (2) mandates that past observations leading to statistically identical futures belong to the same causal state. Let us denote \mathcal{S} as the set of causal states, where each state $s \in \mathcal{S}$ is given by an associated encoding function $s = \epsilon(\vec{r})$. At each time step the ε -machine transitions from causal state j to k whilst emitting an output $r \in \mathcal{R}$, with transition probability $T_{kj}^r = P(R_{t+1} = r, S_{t+1} = k | S_t = j)$. The encoding function enforces *unifilarity* of the ε -machine, where, given the current causal state j and the emitted output symbol r , the subsequent causal state k of the model is uniquely specified [21]. We denote this mapping by a function $\lambda(j, r)$ that outputs the value of the label of the subsequent causal state. This allows us to express

$$T_{kj}^r = P(R_{t+1} = r, S_{t+1} = k | S_t = j) \quad (3)$$

$$= P(r|j) \delta_{k, \lambda(j, r)} \quad (4)$$

where δ_{jk} is the Kronecker- δ function. The amount of information required to track the dynamics of causal states has been widely employed as a measure of structure [20, 39–46], as the *statistical complexity*:

$$C_\mu := - \sum_j P_j \log P_j, \quad (5)$$

where $P_j = \sum_{\vec{r} \in j} P(\vec{r})$ is the steady-state probability of causal state j . The statistical complexity is often compared to the mutual information between the past and future of the system,

$$E = \sum_{\vec{r}, \vec{r}'} P(\vec{r}, \vec{r}') \log \left(\frac{P(\vec{r}, \vec{r}')}{P(\vec{r})P(\vec{r}')} \right). \quad (6)$$

a quantity known as the *excess entropy*. It quantifies the amount of information in the past that correlates with future statistics. The excess entropy (also sometimes called the ‘predictive information’) is also used as a measure of complexity [47, 48]. The data processing inequality [49] ensures that the excess entropy represents a lower bound on the amount of information a simulator of a process must store in any physical theory, and thus $C_\mu \geq E$.

Quantum causal models. Recently, computational mechanics has been extended into the quantum regime [23], where it has been shown that quantum effects allow one to construct causal models that require a lower amount of information than is classically possible. The present state-of-the-art systematic construction methods for quantum models [26, 27] involve step-wise unitary interactions between the model memory and a probe system. The memory of such quantum models store a member of a set of quantum memory states $\{|s_j\rangle\}$

that are in one-to-one correspondence with the causal states of the process. The memory states are then used to produce the future outputs of the process sequentially. Starting from state $|s_j\rangle$ and a blank ancilla, there exists a unitary operator U that satisfies

$$U |s_j\rangle |0\rangle = \sum_{r \in \mathcal{R}} \sqrt{P(r|j)} |s_{\lambda(j,r)}\rangle |r\rangle. \quad (7)$$

The stationary state of the model memory is given by $\rho = \sum_j P_j |s_j\rangle \langle s_j|$, where P_j is as defined for Eq. (5). The amount of information stored internally is given by the von Neumann entropy of ρ :

$$C_q := -\text{Tr}(\rho \log_2 \rho). \quad (8)$$

C_q is referred to as the quantum statistical memory. In general, the memory states are non-orthogonal (i.e., $\langle s_j | s_k \rangle \geq 0$), due to a quantum model being able to encode pasts with partially overlapping futures into partially overlapping states. Therefore, $C_q \leq C_\mu$; a quantum causal model can utilise less memory than the ε -machine of the same process [23–30]. While the quantum models presented here require less memory than ε -machines, they are in general not optimal over all quantum models [30]. However, in certain specific cases, this construction has been shown to be the provably optimal quantum model [31, 37]. C_q thus upper bounds the quantum statistical complexity, and has been suggested as a potential measure of complexity in itself [23, 50].

Measures of complexity. We focus our attention on the following measures of complexity:

- *Statistical complexity* C_μ
- *Quantum statistical memory* C_q
- *Excess entropy* E
- *Half-chain entanglement entropy* $S_{\frac{1}{2}}$

C_μ , C_q , and E have been formally introduced above. The half-chain entanglement entropy of a one-dimensional quantum many-body system quantifies the amount of quantum correlations (entanglement) between the left and right halves of the system [13]. It is defined as

$$S_{\frac{1}{2}} := -\text{Tr}(\rho_A \log_2 \rho_A) = -\text{Tr}(\rho_B \log_2 \rho_B), \quad (9)$$

where $\rho_A = \text{Tr}_B(\rho_{AB})$ and $\rho_B = \text{Tr}_A(\rho_{AB})$ are the density matrices describing the states of the left and right halves of the quantum system respectively. $S_{\frac{1}{2}}$ is measurement basis-independent, and depends only on the state of the quantum many-body system. $S_{\frac{1}{2}}$ is very closely related to the quantum mutual information ($I_q(A, B) = 2S_{\frac{1}{2}}$ for pure states), and is loosely analogous to the excess entropy for quantum processes. Beyond identifying correlations, entanglement has also been suggested as an indicator of critical points of phase transitions in quantum many-body systems [51–53]. However, experimental measurement of $S_{\frac{1}{2}}$ in real quantum systems is a highly non-trivial task [54–57].

III. RESULTS

Stochastic processes from quantum many-body systems. Measurements of quantum systems are inherently probabilistic. When making a series of measurements on quantum systems, the outputs form a stochastic sequence. The structure in this sequence can embody structure present in the underlying quantum state that gave rise to the observations. To this end, we study the structure of infinite length one-dimensional quantum many-body chains, where measurements are made on consecutive sites sweeping from left to right, with spatial position naturally forming an analogue to temporal location. Specifically, we consider non-degenerate, site-local measurement operators such that on site j , a set of measurement outcomes $r_j \in \mathcal{R}$ are associated with unique eigenstates $|r_j\rangle$. This measurement outcome is taken to be the corresponding j -th observation in the constructed stochastic process. As we sweep the output sequence from left to right, it follows then that the output sequence \overleftarrow{r} occurs with probability

$$P(\overleftarrow{r}) = \langle \psi | \bigotimes_{j=-\infty}^{\infty} |r_j\rangle \langle r_j | \psi \rangle \quad (10)$$

where $|\psi\rangle$ is the quantum state of the one-dimensional system being investigated.

Numerical considerations. For numerical tractability, we make two approximations regarding the system size and the measures of complexity. Firstly, rather than an infinite chain, we study large finite-size quantum chains of length N . Secondly, we introduce the truncated Markov memory order L . It represents the number of sites from which past information may be obtained. That is, we approximate $P(r|\vec{r}) \approx P(r|r_{-L:1})$. We take $N \gg L$. We employ tensor network methods [19] (see Appendix) to obtain near exact ground states of the example systems we study, as well as to extract the corresponding measurement sequences that form the stochastic processes.

We now apply our framework to explore the structures of two paradigmatic quantum many-body chains in their respective ground states.

Quantum Ising chain. A quantum Ising chain [58] describes the physics of a system of interacting quantum spins subject to the influence of a magnetic field. They are governed by the Hamiltonian:

$$\mathcal{H}_{QI} = \sum_l -J \sigma_l^x \sigma_{l+1}^x - B \sigma_l^z \quad (11)$$

where J is a coupling parameter, B is the external magnetic field strength, and σ_l^w , $w \in \{x, y, z\}$, are the Pauli operators at site l . The system undergoes a quantum phase transition at $B/J = 0.5$. At $B \gg J$, the field along the z -direction dominates the correlations in the system; the ground state of the system is $|\psi_g\rangle = |\dots \downarrow_{i-1} \downarrow_i \downarrow_{i+1} \dots\rangle$, fully-polarised along the z -axis. On

the other hand, when $B \ll J$, the field is much weaker than the spin-spin correlation along the x -direction. There are then two degenerate ground states, with all spins either parallel or anti-parallel with the x -axis, $|\psi_g\rangle = |\cdots \rightarrow_{i-1} \rightarrow_i \rightarrow_{i+1} \cdots\rangle$ or $|\cdots \leftarrow_{i-1} \leftarrow_i \leftarrow_{i+1} \cdots\rangle$.

We investigate the structure of the model at a range of truncated Markov memory orders $L \in \{1, 3, 5, 7, 9\}$, with $N = 500$. The causal states are then determined by the L rightmost spins of the past spins, as defined in Eq. (2). We find that each length L spin configuration belongs to a unique causal state. To ensure that there is no spurious splitting of causal states, we determine that the conditional probability distributions differ by more than $\mathcal{O}(10^{-12})$ from each other, while the ground states $|\psi_g\rangle$ are accurate to $\mathcal{O}(10^{-14})$; that the error in the ground state is significantly smaller than the distance between conditional distributions of the spin configurations.

Using the framework above, we study the structural complexity of the quantum Ising chain through its measurement sequences as obtained from σ_θ -basis measurements, where

$$\sigma_\theta = \begin{pmatrix} \cos \theta & \sin \theta \\ \sin \theta & -\cos \theta \end{pmatrix}, \quad (12)$$

with $\theta \in [0, \pi/2]$ the angle measured from the z -axis of the Bloch sphere. Angles $\theta = 0$ and $\theta = \pi/2$ correspond to the z - and x -axes respectively. Intuitively, σ_z measurement in the $B \gg J$ regime will result in a highly-ordered stochastic process, while σ_x will return a near-random process. Conversely in the $B \ll J$ regime, measurement sequences along σ_z will yield a near-random stochastic process, while σ_x will result in a highly-ordered process.

Fig. 1 compares C_μ , C_q , E , and $S_{\frac{1}{2}}$ for measurements of σ_x and σ_z at different B/J , where we observe interesting differences between these measures of structure and complexity. Firstly, in all measurement bases studied, C_q , E , and $S_{\frac{1}{2}}$ reach maximal values close to the phase transition $B/J \approx 0.5$. Instead, C_μ exhibits its largest gradient near the phase transition.

We also observe that $S_{\frac{1}{2}} > C_q$ for all measurement bases. This is because projecting a quantum state onto a specific basis effectively destroys information about other measurement bases, while $S_{\frac{1}{2}}$ is a quantity that takes into account the full information contained in the quantum state. The relation $S_{\frac{1}{2}} > C_q$ highlights that simulating a quantum system measured in a specific basis can require less information than the quantum correlations present in the system. This highlights that if we don't require replication of all measurement bases, the state is not the most efficient simulator of itself.

Fig. 1 also shows that when sequences from measurement outcomes of the quantum Ising chain are more ordered ($B \gg J$ for σ_z -basis, $B \ll J$ for σ_x -basis), the corresponding values of C_μ , C_q , and E are lower. In a highly-ordered stochastic process, the corresponding ε -machine consists of a single dominant causal state that is occupied with very high probability, and other causal

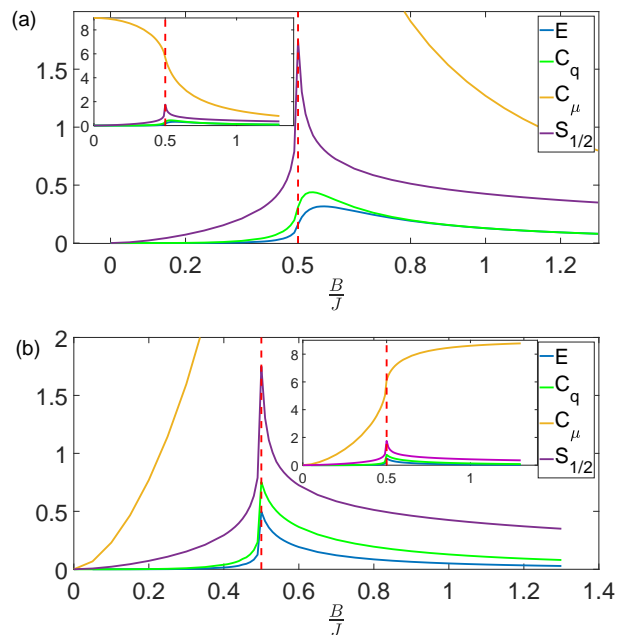


FIG. 1: Comparison between E , C_q , C_μ in the (a) σ_z , and (b) σ_x measurement bases, and $S_{\frac{1}{2}}$ of the one-dimensional quantum Ising system for $L = 9$. The vertical dashed line demarcates the phase transition of the system.

states arise with very low probabilities. Thus the resulting ε -machine requires little information to be stored to accurately simulate the corresponding stochastic process. Our quantum model behaves similarly in this regime, hence C_q mirrors C_μ . Further, in this parameter regime the more ordered the sequences are, the less information is carried forward from the left half to the right half of the system, resulting in low values of E .

On the other hand, when the observation sequences are near-random ($B \gg J$ for σ_x -basis, $B \ll J$ for σ_z -basis), C_μ exhibits drastically different qualitative behaviour compared to C_q and E , as seen in Fig. 1. Both C_q and E are lower when the sequences appear more random, unlike C_μ , which saturates in this regime. This is because in the near-random limit the past configurations have different-yet-strongly-overlapping conditional future probability distributions, and thus they are mapped into different causal states. As a classical model, the ε -machine can only store information in distinguishable states, despite multiple causal states having significantly overlapping conditional future statistics; consequently, C_μ is high in this regime. In contrast, quantum models have the ability to store information in non-orthogonal states. Thus, causal states with highly-overlapping future conditional probability distributions will be encoded into highly-overlapping quantum states, resulting in low C_q in the near-random regime.

We also observe differing behaviour of C_μ and C_q with respect to the truncated Markov memory order, as illustrated in Figs. 2 and 3. As L is increased, C_q also in-

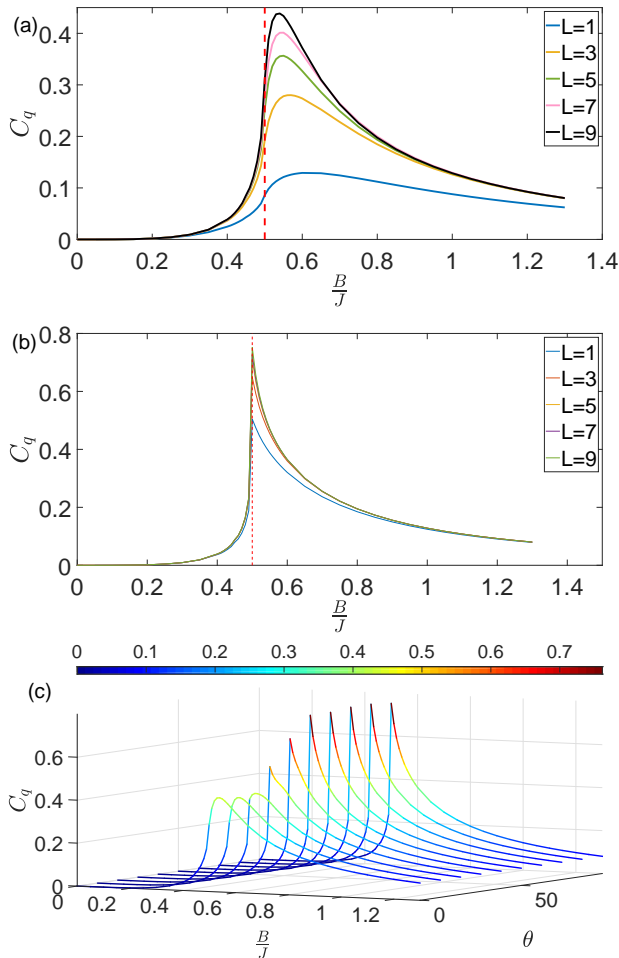


FIG. 2: C_q plotted against B/J for sequences of measurements of the quantum Ising chain along (a) σ_z , (b) σ_x , and (c) σ_θ for multiple values of θ . The vertical dashed lines in (a) and (b) demarcate the phase transition of the system.

creases, but at a decreasing rate, indicating that the value of C_q converges as larger L is considered [Fig. 2]. This is consistent with the decrease in correlation strength between spins when the distance between them increases (i.e., spins that are further apart are more weakly correlated). This means that at high L , increasing the Markov memory order further adds little predictive information. This cannot be utilised effectively by the classical ε -machine with access only to orthogonal states; as L increases, so too does the number of causal states – resulting in a higher C_μ , as illustrated by Fig. 3.

We see that the behaviour of C_μ with respect to B/J changes as we rotate the measurement angle θ from σ_z to σ_x [Fig. 3(c)]. As θ changes from 0 to $\pi/2$, the measurement outcome sequences sweep between near-random and near-deterministic in the region $B \ll J$, and between near-deterministic and near-random in the region $B \gg J$. Fig. 2(c) shows the counterpart behaviour of C_q with respect to the different measurement angles. As the measurement basis changes from σ_z to σ_x , we observe

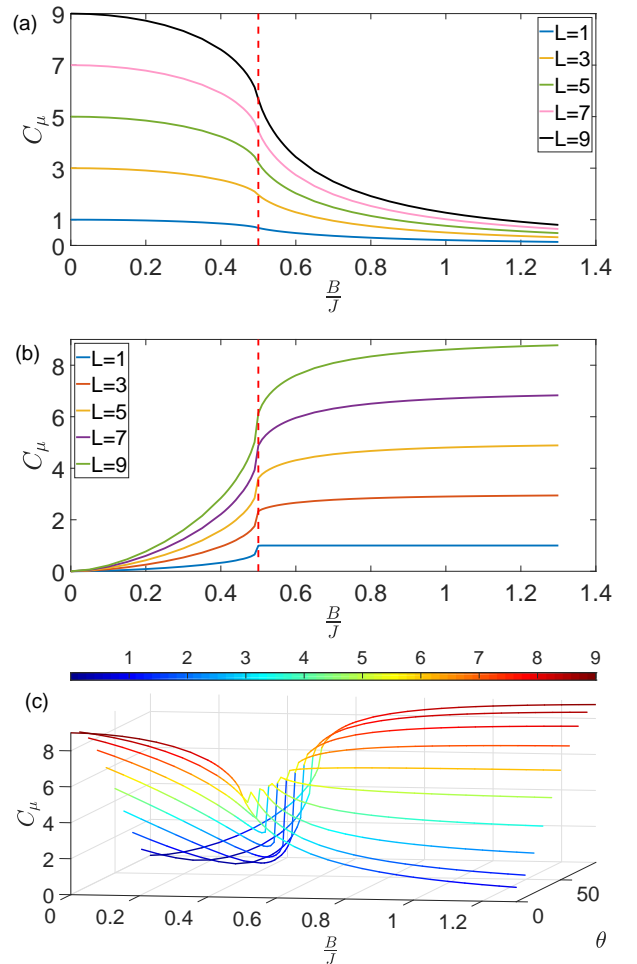


FIG. 3: C_μ plotted against B/J for sequences of measurements of the quantum Ising chain along (a) σ_z , (b) σ_x , and (c) σ_θ for multiple values of θ . The vertical dashed lines in (a) and (b) demarcate the phase transition of the system.

that the peak of C_q increases with respect to σ_θ . In the parameter region that is neither random nor deterministic, our quantum model stores less information than when measured in a basis that is closer to the z -axis. This captures the underlying structure of the quantum Ising chain very well, as measurement outcomes along the z -axis are less dependent on the past spins, because the inter-spin coupling of the system is along the x -axis.

Bose-Hubbard chain. We now look at structure in the one-dimensional Bose-Hubbard model, which describes the physics of interacting spinless bosons on a lattice [3, 5, 6]. It is governed by:

$$\mathcal{H}_{BH} = -J \sum_l b_l^\dagger b_{l+1} + \text{h.c.} + \frac{U}{2} \sum_l n_l(n_l - 1), \quad (13)$$

where b_l^\dagger and b_l are bosonic creation and annihilation operators and $n_l = b_l^\dagger b_l$ is the number of bosons at site l . The variable J denotes the hopping amplitude, describing the kinetic energy of the bosons, and U is the

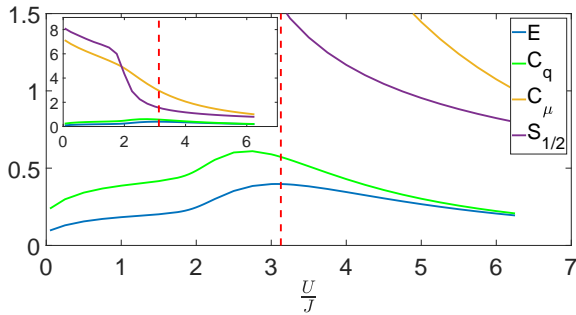


FIG. 4: E , C_q and C_μ at $L = 4$, and $S_{\frac{1}{2}}$, plotted against U/J , for sequences of measurements of n in the Bose-Hubbard chain. The vertical dashed line demarcates the phase transition of the system.

on-site repulsive interaction strength. The filling factor ν is defined as the average number of bosons per site; we consider a chain with $\nu = 1$. In our numerical calculations, we use $N = 300$ and truncated Markov memory orders of $L \in \{1, 2, 3, 4\}$. We also enforce that each site has a maximum occupation number $n_{\max} = 4$ – higher values of occupation number have very low probability of occurrence (and thus have little impact on the state), yet demand significantly more computational power. In the ground state, when $J \gg U$ all bosons occupy zero-momentum eigenstates, wherein they are completely delocalised across the lattice; this is the superfluid phase. On the other hand, when $J \ll U$, the system is in the Mott insulator phase, where at integer filling factors ν , each site contains ν highly-localised bosons. The one-dimensional Bose-Hubbard model undergoes a quantum phase transition at $U/J \approx 3.1$ [6, 59] for the case of $\nu = 1$.

We calculate the structural complexity measures for measurement outcome sequences of the Bose-Hubbard chain in the number basis, wherein n is measured sequentially on every site. Fig. 4 shows the behaviour of C_μ , C_q , and E for these sequences, as well as $S_{\frac{1}{2}}$. We observe that E peaks close to the phase transition, while C_q peaks earlier. This indicates that E may identify the phase transition, while C_q and C_μ do not. This is in contrast to the quantum Ising chain, where both E and C_q (in multiple measurement bases) reach a maximum value in the vicinity of the phase transition.

In the superfluid phase ($J \gg U$) C_μ behaves very differently to C_q and E : C_μ increases as $U/J \rightarrow 0$, while C_q and E decrease. This is because the bosons are delocalised, leading to near-random measurement sequences for the site occupations. Hence, the models occupy all available (quantum) causal states with almost equal probabilities. Analogous to the quantum Ising chain however, C_μ and C_q behave very differently, due to the (non-)orthogonality of (quantum) memory states.

On the other hand, in the Mott insulator phase ($J \ll U$), C_μ , C_q , and E decrease as U/J increases. In this regime, the bosons in the system are highly localised, and so measurement in the n -basis yields a highly-ordered

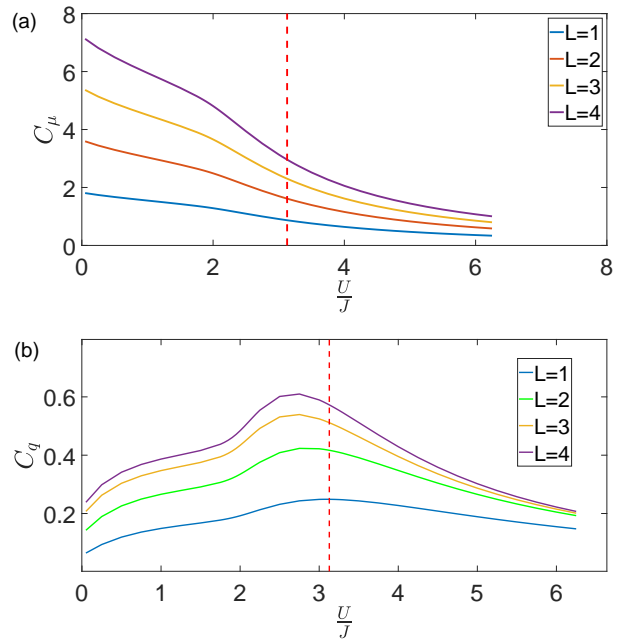


FIG. 5: Scaling with L of (a) C_μ and (b) C_q against U/J for sequences of measurements of n in the Bose-Hubbard chain. The vertical dashed lines demarcate the phase transition of the system.

stochastic process since the number of bosons at each site tends to ν as $U/J \rightarrow \infty$. Similar to the analogous limit in the quantum Ising chain, measurement sequences that are highly-ordered have a single causal state that manifests with very high probability, while other causal states all occur with low probabilities. This results in low values of both C_μ and C_q .

Fig. 4 also shows that $S_{\frac{1}{2}}$ is larger than C_q for the measurement outcome sequences; as with the quantum Ising chain, this is because $S_{\frac{1}{2}}$ quantifies the full quantum correlations between two halves of the system, while C_q results from projecting the quantum state onto one specific basis, and discarding information about all other bases. Notably, in the superfluid parameter region $S_{\frac{1}{2}}$ behaves very differently to C_q and E : $S_{\frac{1}{2}}$ increases, while C_q and E decrease. This is because projecting the state into the n -basis removes the structure in the conjugate basis (i.e., momentum), that would have manifest large half-chain entanglement.

Finally, Fig. 5 shows how C_μ and C_q scale with increasing L . As with the quantum Ising chain, we see that C_q displays signs of convergence as L is increased, while C_μ does not. Again, this is due to the decay in the strength of correlations between site occupations with increasing distance.

IV. DISCUSSION

Our results shows that classical and quantum measures of structural complexity can exhibit drastically different qualitative behaviour when applied to sequences generated by measurement outcomes of quantum systems. In particular, it is evident that the measures interpret near-randomness very differently; quantum models are typically able to capture the predictive features in near-random sequences without storing a large amount of information about the past, in contrast to corresponding minimal classical models. The quantum measures also appear to signal proximity to a phase transition – an interesting future work in this direction is the study of universality classes of quantum systems – can quantum systems be categorised into universality classes according to their structural complexities? Members of the same universality class have identical critical behaviour despite possibly having radically diverse microscopic behaviour.

Moving forward in the field of computational mechanics, the transducer framework [60, 61] provides a natural extension to study quantum systems as input-output processes, and thus lines up as a natural next step to this work. In such processes, the choice of the measurement basis would form the input, and the resulting measurement sequence is the output, allowing for the fully-quantum nature of non-commuting measurements to be considered. It would be interesting to make this extension and study the dynamics of quantum processes by measuring them at different bases at different timesteps, capturing the structure and complexity within an evolving quantum system. An ultimate goal of quantum computational mechanics is to construct quantum causal models that can simulate any quantum stochastic processes without restriction in choice of measurement bases; the results in this manuscript serve as a crucial first step towards this direction.

Acknowledgements. We thank Felix Binder, Yang Chengran, Jirawat Tangpanitanon, and Benjamin Yadin for enlightening discussion, and the University of Oxford Advanced Research Computing department for providing us with access to their platform to run our numerical simulations. We are also grateful to Sarah Al-Assam, Stephen Clark, and Dieter Jaksch for their permission to use their tensor network library [62]. This work was funded by the Lee Kuan Yew Endowment Fund (Postdoctoral Fellowship), Singapore Ministry of Education Tier 1 grant RG190/17, FQXi, Singapore National Research Foundation Fellowship NRF-NRFF2016-02, and NRF-ANR grant NRF2017-NRF-ANR004 VanQuTe, and the the FQXi Large Grant: The role of quantum effects in simplifying adaptive agents. T.J.E. thanks the Centre for Quantum Technologies for their hospitality.

TECHNICAL APPENDIX

Tensor Network Theory (TNT) [62] is a set of powerful and efficient numerical methods for classically simulating quantum many-body systems. In this Appendix, we briefly review matrix product states (MPS), matrix product operators (MPO), and the density matrix renormalisation group (DMRG) in the context of our work. MPS and MPO provide efficient descriptions of states and operators of quantum many-body systems respectively, while DMRG is an iterative procedure that variationally minimises the energy of Hamiltonians to obtain the ground states of quantum many-body systems.

MPS [18] are widely used as efficient representations of low energy states of one-dimensional quantum systems. In a quantum many-body chain, each lattice site is represented by a tensor, and the tensors are connected to their neighbours. Consider a quantum many-body chain of size N in a quantum state

$$|\psi\rangle = \sum_{i_1 i_2 \dots i_N} c_{i_1 i_2 \dots i_N} |i_1\rangle |i_2\rangle \dots |i_N\rangle \quad (14)$$

where $\{|i_j\rangle\}$ are the local orthonormal basis states. We can perform repeated Schmidt decompositions [49] at each site, splitting the tensor $c_{i_1 i_2 \dots i_N}$ into local tensors $\Gamma^{[j]}$, and Schmidt coefficients $\lambda^{[j]}$ that quantify the entanglement across the split, which gives us the canonical form of the MPS representation of the state:

$$|\psi\rangle = \sum_{\{i\}, \{\alpha\}} \left(\Gamma_{\alpha_1}^{[1] i_1} \lambda_{\alpha_1}^{[1]} \Gamma_{\alpha_1 \alpha_2}^{[2] i_2} \lambda_{\alpha_2}^{[2]} \dots \lambda_{\alpha_{N-1}}^{[N-1]} \Gamma_{\alpha_{N-1}}^{[N] i_N} \right) |i_1\rangle |i_2\rangle \dots |i_N\rangle, \quad (15)$$

where α_j takes positive integer values up to the rank of $\Gamma^{[j]}$. By contracting the Schmidt coefficient tensors $\lambda^{[j]}$ into the local tensors $\Gamma^{[j]}$, we obtain a more generic form:

$$|\psi\rangle = \sum_{i_1 i_2 \dots i_N} A^{x_1} A^{x_2} \dots A^{x_N} |i_1\rangle |i_2\rangle \dots |i_N\rangle, \quad (16)$$

where A^{x_j} is a matrix with the same dimension as the local basis states.

In a similar fashion, a quantum operator can be written in the form of MPO [63]:

$$\mathcal{H} = \sum_{i,k} H^{i_1, k_1} H^{i_2, k_2} \dots H^{i_N, k_N} |i_1 i_2 \dots i_N\rangle \langle k_1 k_2 \dots k_N|, \quad (17)$$

where H^{i_j, k_j} is a matrix with the dimension of the local basis state. With quantum states and Hamiltonians represented in MPS and MPO forms respectively, ground states $|\psi_g\rangle$ may then be obtained by minimising $\langle \psi | \mathcal{H} | \psi \rangle$ across all states using the DMRG algorithm.

The DMRG algorithm [64, 65] is an iterative, variational method that truncates the degrees of freedom of the system, retaining only the most significant features required to accurately describe the physics of a target state. The algorithm achieves remarkable precision

in describing one-dimensional quantum many-body systems [66].

In the DMRG algorithm, the elementary unit is a site, described by the state d_i where $i = 1, \dots, D$ is the label of the states accessible to a given site. A block $B(L, v_L)$ consists of L sites, and has total dimension v_L ; H_B is the Hamiltonian of the block, containing only terms that involve the sites inside the block. Whenever a block is enlarged, a site is added to the block, forming an enlarged block B^e with a Hilbert space dimension that is the product of the Hilbert space of $B(L, v_L)$ and a site, i.e. $v_L \times D$. An important step in the algorithm is the formation of superblock Hamiltonians, consisting of two enlarged blocks connected to each other. The superblock ground state is calculated using Lanczos [67] or Davidson [68] methods. The ground state is then truncated by discarding the least-probable eigenstates.

The algorithm itself consist of two parts: the warm-up cycle, and finite-system algorithm. The warm-up cycle is designed to create a system block of the desired length of at most dimension χ , before the finite-system algorithm is applied to compute the ground state. Starting from a block $B(1, D)$, each step of the warm-up cycle is carried out as follows [69]:

1. Start from a left block $B(L, v_L)$, and enlarge the block by adding a single site.
2. Form a superblock by adding a reflected copy of the enlarged block to its right.
3. Obtain the ground state of the superblock, and the $v_{l+1} = \min(v_l D, \chi)$ eigenstates of the reduced density matrix of the left enlarged block with largest

eigenvalues.

4. The truncated left enlarged block is used for the next iteration.
5. Renormalise all operators to obtain block $B(L + 1, v_{L+1})$.

These steps are repeated until the desired length L_{\max} is reached. Once the infinite-system algorithm reaches the desired length, the system consist of two blocks of $B(L_{\max}/2 - 1, \chi)$ and two free sites. The subsequent step is called the “sweep procedure”, the goal of which is to enhance the convergence of the target state. The sweep procedure consists of enlarging the left block with one site and reducing the right block correspondingly to keep the length fixed. While the left block is constructed by the usual enlarging steps, the right block is recalled from memory, as it has been built in the infinite-system algorithm and saved. This procedure is repeated until the left block reaches the length $L_{\max} - 4$. At this point the right block $B(1, D)$ with one site is constructed from scratch and the left block $B(L_{\max}, \chi)$ is obtained through renormalisation. The sweep procedure is then repeated from right to left, and at each iteration, the renormalised block has to be stored in memory. The procedure is stopped when the system energy converges.

In this manuscript, we use the implementations of these algorithms as described in [62], and the ground states are computed with $\chi = 150$ for the one-dimensional quantum Ising chain, and $\chi = 80$ for the one-dimensional Bose-Hubbard chain. The resulting ground states are accurate up to $\mathcal{O}(10^{-14})$.

-
- [1] R. P. Feynman, International Journal of Theoretical Physics **21**, 467 (1982).
- [2] I. Bloch, J. Dalibard, and S. Nascimbene, Nature Physics **8**, 267 (2012).
- [3] M. Lewenstein, A. Sanpera, and V. Ahufinger, *Ultracold Atoms in Optical Lattices: Simulating Quantum Many-Body Systems* (Oxford University Press, Oxford, England, 2012).
- [4] T. H. Johnson, S. R. Clark, and D. Jaksch, EPJ Quantum Technology **1**, 1 (2014).
- [5] D. Jaksch, C. Bruder, J. I. Cirac, C. W. Gardiner, and P. Zoller, Physical Review Letters **81**, 3108 (1998).
- [6] M. Greiner, O. Mandel, T. Esslinger, T. W. Hänsch, and I. Bloch, Nature **415**, 39 (2002).
- [7] D. Jaksch and P. Zoller, New Journal of Physics **5**, 56 (2003).
- [8] I. Bloch, J. Dalibard, and W. Zwerger, Rev. Mod. Phys. **80**, 885 (2008).
- [9] K. Baumann, C. Guerlin, F. Brennecke, and T. Esslinger, Nature **464**, 1301 (2010).
- [10] H. Ritsch, P. Domokos, F. Brennecke, and T. Esslinger, Reviews of Modern Physics **85**, 553 (2013).
- [11] M. Aidelsburger, M. Atala, M. Lohse, J. T. Barreiro, B. Paredes, and I. Bloch, Physical Review Letters **111**, 185301 (2013).
- [12] H. Miyake, G. A. Siviloglou, C. J. Kennedy, W. C. Burton, and W. Ketterle, Physical Review Letters **111**, 185302 (2013).
- [13] L. Amico, R. Fazio, A. Osterloh, and V. Vedral, Reviews of Modern Physics **80**, 517 (2008).
- [14] R. Horodecki, P. Horodecki, M. Horodecki, and K. Horodecki, Reviews of Modern Physics **81**, 865 (2009).
- [15] G. Vidal, Physical Review Letters **91**, 147902 (2003).
- [16] F. Verstraete and J. I. Cirac, Physical Review B **73**, 094423 (2006).
- [17] U. Schollwöck, Annals of Physics **326**, 96 (2011).
- [18] R. Orús, Annals of Physics **349**, 117 (2014).
- [19] M. A. Valdez, D. Jaschke, D. L. Vargas, and L. D. Carr, Physical Review Letters **119**, 225301 (2017).
- [20] J. P. Crutchfield and K. Young, Physical Review Letters **63**, 105 (1989).
- [21] C. R. Shalizi and J. P. Crutchfield, Journal of Statistical Physics **104**, 817 (2001).
- [22] J. P. Crutchfield, Nature Physics **8**, 17 (2012).
- [23] M. Gu, K. Wiesner, E. Rieper, and V. Vedral, Nature Communications **3**, 762 (2012).

- [24] J. R. Mahoney, C. Aghamohammadi, and J. P. Crutchfield, *Scientific Reports* **6**, 20495 (2016).
- [25] M. S. Palsson, M. Gu, J. Ho, H. M. Wiseman, and G. J. Pryde, *Science Advances* **3**, e1601302 (2017).
- [26] C. Aghamohammadi, S. P. Loomis, J. R. Mahoney, and J. P. Crutchfield, *Physical Review X* **8**, 011025 (2018).
- [27] F. C. Binder, J. Thompson, and M. Gu, *Physical Review Letters* **120**, 240502 (2018).
- [28] T. J. Elliott and M. Gu, *npj Quantum Information* **4**, 18 (2018).
- [29] T. J. Elliott, A. J. P. Garner, and M. Gu, arXiv preprint arXiv:1803.05426 (2018).
- [30] Q. Liu, T. J. Elliott, F. C. Binder, C. Di Franco, and M. Gu, arXiv preprint arXiv:1810.09668 (2018).
- [31] W. Y. Suen, J. Thompson, A. J. P. Garner, V. Vedral, and M. Gu, *Quantum* **1**, 25 (2017).
- [32] C. Aghamohammadi, J. R. Mahoney, and J. P. Crutchfield, *Physics Letters A* **381**, 1223 (2017).
- [33] F. G. Jouneghani, M. Gu, J. Ho, J. Thompson, W. Y. Suen, H. M. Wiseman, and G. J. Pryde, arXiv preprint arXiv:1711.03661 (2017).
- [34] S. Loomis and J. P. Crutchfield, arXiv preprint arXiv:1808.08639 (2018).
- [35] A. J. Garner, Q. Liu, J. Thompson, V. Vedral, et al., *New Journal of Physics* **19**, 103009 (2017).
- [36] C. Aghamohammadi, J. R. Mahoney, and J. P. Crutchfield, *Scientific Reports* **7**, 6735 (2017).
- [37] J. Thompson, A. J. P. Garner, J. R. Mahoney, J. P. Crutchfield, V. Vedral, and M. Gu, *Physical Review X* **8**, 031013 (2018).
- [38] A. Khintchine, *Mathematische Annalen* **109**, 604 (1934).
- [39] J. P. Crutchfield and D. P. Feldman, *Physical Review E* **55**, 1239R (1997).
- [40] A. J. Palmer, C. W. Fairall, and W. A. Brewer, *IEEE Transactions on Geoscience and Remote Sensing* **38**, 2056 (2000).
- [41] D. P. Varn, G. S. Canright, and J. P. Crutchfield, *Physical Review B* **66**, 174110 (2002).
- [42] R. W. Clarke, M. P. Freeman, and N. W. Watkins, *Physical Review E* **67**, 016203 (2003).
- [43] J. B. Park, J. W. Lee, J.-S. Yang, H.-H. Jo, and H.-T. Moon, *Physica A: Statistical Mechanics and its Applications* **379**, 179 (2007).
- [44] C.-B. Li, H. Yang, and T. Komatsuzaki, *Proceedings of the National Academy of Sciences* **105**, 536 (2008).
- [45] R. Haslinger, K. L. Klinkner, and C. R. Shalizi, *Neural Computation* **22**, 121 (2010).
- [46] D. Kelly, M. Dillingham, A. Hudson, and K. Wiesner, *PloS one* **7**, e29703 (2012).
- [47] R. Shaw, *The dripping faucet as a model chaotic system* (Aerial Press, 1984).
- [48] W. Bialek, I. Nemenman, and N. Tishby, *Neural Computation* **13**, 2409 (2001).
- [49] M. A. Nielsen and I. L. Chuang, *Quantum computation and quantum information* (Cambridge University Press, 2010).
- [50] R. Tan, D. R. Terno, J. Thompson, V. Vedral, and M. Gu, *The European Physical Journal Plus* **129**, 1 (2014).
- [51] A. Osterloh, L. Amico, G. Falci, and R. Fazio, *Nature* **416**, 608 (2002).
- [52] T. J. Osborne and M. A. Nielsen, *Physical Review A* **66**, 032110 (2002).
- [53] G. Vidal, J. I. Latorre, E. Rico, and A. Kitaev, *Physical Review Letters* **90**, 227902 (2003).
- [54] A. J. Daley, H. Pichler, J. Schachenmayer, and P. Zoller, *Physical Review Letters* **109**, 020505 (2012).
- [55] D. A. Abanin and E. Demler, *Physical Review Letters* **109**, 020504 (2012).
- [56] R. Islam, R. Ma, P. M. Preiss, M. E. Tai, A. Lukin, M. Rispoli, and M. Greiner, *Nature* **528**, 77 (2015).
- [57] T. J. Elliott, W. Kozłowski, S. F. Caballero-Benitez, and I. B. Mekhov, *Physical Review Letters* **114**, 113604 (2015).
- [58] D. C. Mattis, *The Theory of Magnetism Made Simple: An Introduction to Physical Concepts and to Some Useful Mathematical Methods* (World Scientific, 2006).
- [59] M. Pino, J. Prior, A. M. Somoza, D. Jaksch, and S. R. Clark, *Physical Review A* **86**, 023631 (2012).
- [60] N. Barnett and J. P. Crutchfield, *Journal of Statistical Physics* **161**, 404 (2015).
- [61] J. Thompson, A. J. P. Garner, V. Vedral, and M. Gu, *npj Quantum Information* **3**, 6 (2017).
- [62] S. Al-Assam, S. R. Clark, and D. Jaksch, *Journal of Statistical Mechanics: Theory and Experiment* **2017**, 093102 (2017).
- [63] B. Pirvu, V. Murg, J. I. Cirac, and F. Verstraete, *New Journal of Physics* **12**, 025012 (2010).
- [64] S. R. White, *Physical Review Letters* **69**, 2863 (1992).
- [65] S. R. White, *Physical Review B* **48**, 10345 (1993).
- [66] S. R. White and D. A. Huse, *Physical Review B* **48**, 3844 (1993).
- [67] C. Lanczos, *An iteration method for the solution of the eigenvalue problem of linear differential and integral operators* (United States Governm. Press Office Los Angeles, CA, 1950).
- [68] E. R. Davidson, *Journal of Computational Physics* **17**, 87 (1975).
- [69] G. De Chiara, M. Rizzi, D. Rossini, and S. Montangero, *Journal of Computational and Theoretical Nanoscience* **5**, 1277 (2008).